Bull Mater Sci (2020) 43:279
https://doi.org/10.1007/s12034-020-02255-8

Formation of diamond nanostructures from graphite using 10 W fibre laser

ASSIM VERMA, BHANU PRAKASH and DEEPIKA SHARMA*
Institute of Nano Science and Technology, Mohali 160062, India
*Author for correspondence (deepika@inst.ac.in)

MS received 13 April 2020; accepted 11 August 2020

Abstract. The high activation energy required for graphite–diamond transition limits its applicability in novel areas. To exploit fully the multifunctional properties of diamond in diverse fields, there is a necessity to explore more efficient ways for its synthesis. In this study, we have demonstrated a new approach for nanodiamonds formation by employing a commercially available low power 10 W continuous-wave fibre laser. The laser system is modulated to generate the high-pressure high temperature environment necessary for the phase conversion of graphite to diamond. The microsecond pulse duration combined with liquid confinement effect on plasma provide scope for a lower rate of supercooling, which restricts the epitaxial growth of the crystals. The sample is characterized by X-ray powder diffraction, transmission electron microscope and Raman spectroscopy, confirming the presence of different types of nanodiamonds including newly discovered n-diamond. The process offers many important advantages like scalable process, non-catalyst-based eco-friendly and cost-effective synthesis of metastable nanodiamonds. The results demonstrate the effectuality of inexpensive commercial lasers towards attaining the localized extreme environment necessary for direct phase conversion of diamond materials.

Keywords. Nanodiamond; laser ablation; allotropes; phase conversion; green synthesis; fibre laser.

1. Introduction

Diamond is the special allotrope of carbon having closest atomic packing (176 atoms nm^{-3}) and exist from nano to macro scale. The high atomic density combined with the maximum number of equidistant covalent bonds among carbon atoms (4) results in the enormous bond strength of 7.4 eV. This strong atomic bonding is responsible for its extreme physical, chemical, electronical and optical properties. The combination of these properties in a single allotrope of carbon makes it a wonder material, which finds its way in many emerging technologies like diamond batteries [1], fuel cells [2], quantum computing [3], quantum sensing [4], particle detector [5], theranostics [6], etc.

After the discovery of nanodiamonds in the 1960s [7], various synthesis routes have been developed like high-pressure high temperature carbon vapour deposition (HPHT CVD) [8], microwave plasma carbon vapour deposition (MPCVD) [9], ultrasonic cavitation method [10], detonation synthesis [11] and pulse laser ablation in liquid (PLAL) [12]. Each route has its advantage and disadvantage, which strongly influence the properties of nanodiamond [13]. Nevertheless, the requirement of very high activation energy for graphite to diamond phase transition makes it difficult to synthesize by efficient means mainly due to the inherent cost associated in keeping the environment in extreme conditions. PLAL-assisted nanodiamond synthesis has gained immense popularity in past decades, because first, the laser is an efficient source of energy capable of heating material to thousands of Kelvin in a very short time frame, and second, laser ablation in liquid has been considered as a favourable process for graphite–diamond transformation.

According to the phase diagram of carbon, the conversion of graphite to diamond takes place in the HPHT region i.e., 1600–2500 K at 15 GPa [14]. This has been previously achieved by PLAL experiments using high power pulsed lasers [15–20], despite the wide-scale availability of continuous wave-type lasers mainly due to the crucial effect of rapid quenching of carbon plume after laser irradiation on the formation of diamond crystals. The laser shot heat the target instantly giving rise to the carbon plume and water layer plays an equally important role by confining the high-energy carbon plume and rapidly quenching it [21]. The quenching rate is enormous and depending upon various experimental parameters, it varies from 10^5 to 10^{17} K s^{-1} leading to different types of crystal structures [22]. The utilization of pulsed laser with pulse width ranging from low 25 fs to as high as 1.2 ms has been previously shown to produce nanodiamonds of various types and sizes. Laser parameters like wavelength and intensity also play a crucial role in the type and size of crystals [15–20].

Published online: 15 October 2020

Fibre lasers are more efficient, eco-friendly and economical sources of energy than pulsed lasers. They also exhibit superior beam quality due to minimum beam propagation ratio (M^2 value) and also comprise of all solid-state immovable components leading to high reliability and low maintenance cost due to no wear and tear [23]. In an attempt to explore a novel, environment friendly and cost-effective approach to synthesize diamond material, we employed a commercially available 10 W CW fibre laser to achieve the localized HPHT conditions vital for the formation of diamond crystals from graphite. The parameters of laser were set to produce highly energetic plasma at solid–liquid interface followed by slow undercooling to promote diamond nucleation. Characterization of the sample resulted in the identification of nanodiamonds having different morphologies, including n-diamond that is discussed in detail in the results section.

2. Materials and methods

The experimental setup is shown in figure 1. A graphite pellet is used as the starting material by compressing high-purity graphite powder at 120 kg cm^{-2} using a hydraulic press to make a solid pellet. This pellet was then suspended in a beaker with deionized water such that the water level is not more than 2–3 mm above the upper surface of the pellet. The pellet was targeted by continuous wave fibre laser (Trotec speedy 100 flexx) having wavelength, power and frequency 1064 nm, 10 W and 80,000 Hz, respectively. To ablate the graphite pellet we used some random pattern with hairline thickness, as these engravers work on graphics design input. The whole process was repeated for 30 min and the left-out pellet was discarded. The solution was dried in an oven at 80°C to prevent bubble formation and splashes.

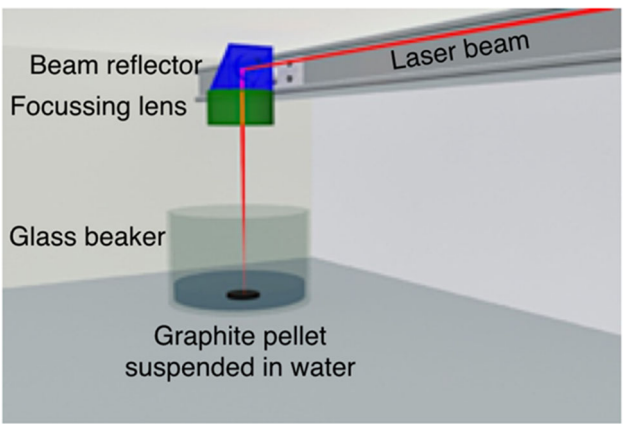

Figure 1. Graphical illustration of experimental setup.

2.1 *Sample characterization*

X-ray powder diffraction (XRD) measurements were performed on a Bruker D8 diffractometer using Ni-filtered Cu Kα source (λ = 1.5418 Å), with an accelerating voltage of 40 kV and electric current of 30 mA. High-resolution images of ablated sample were taken using high-resolution transmission electron microscope (HRTEM) JEOL-JEM2100, equipped with an Orius camera in-line (Gatan, Pleasanton, CA, USA) with accelerating voltage of 200 kV using lanthanum hexaboride filament. The sample was first purified by thermal oxidation of graphitic content at 420°C for 120 h in a furnace as described by Pichot *et al* [24]. The resultant sample was dispersed in alcohol followed by drop-casting onto carbon-coated 300 mesh copper grid and drying in vacuum. For Raman spectroscopy, the purified sample was dispersed in alcohol and drop casted on glass slide until completely dry and performed using confocal Raman spectrometer (WITec Focus innovations) with 532 nm Nd:YAG laser at 600 line mm^{-1} grating. The sample was excited by the unpolarized laser beam of 1 μm spot size with a numerical aperture (NA) of 0.9 and a spectral resolution of 0.1 cm^{-1}.

3. Results and discussion

The fibre laser was run on the submerged target for 15 min. The power density and fluence of laser used in the present work are approximately 12.7 × 10^6 W cm^{-2} and 158.7 J cm^{-2}, respectively. When a high fluence laser is focussed on the graphite target exceeding its damage threshold (55 J cm^{-2}) [25], the high energy photons get absorbed by the graphite layer due to inverse bremsstrahlung and photo-ionization, which give rise to the plasma plume at the solid–liquid interface [21]. As more and more carbon atoms are energized during laser irradiation, the plasma

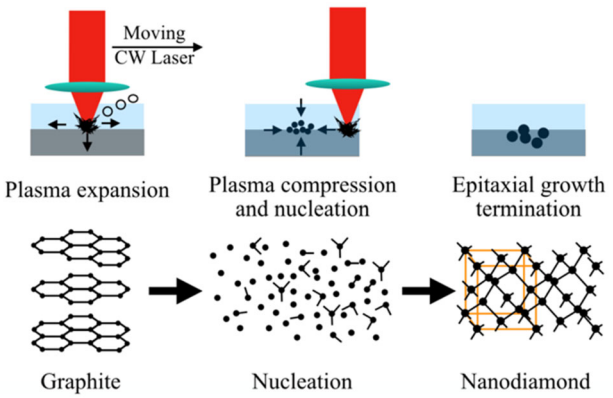

Figure 2. Schematic of phase transformation from graphite to nanodiamond. During irradiation of graphitic target plasma expands. Post irradiation rapid compression of plasma plume takes place. The rapid compression promotes epitaxial growth on diamond nucleation site.

expands quickly as illustrated in figure 2. After irradiation, this expansion of plasma undercools quickly due to liquid confinement effect and parasitic plasma formation around the irradiated spot, resulting in the rapid quenching of reactive carbon species in plasma [26]. In this high pressure–temperature (*P–T*) region, diamond becomes the stable phase of carbon [21,27]. The rate of undercooling affects the growth velocity and thus the size of the diamond nucleus. Ultra-rapid quenching at a rate of $V \approx 10^{13}$ K s^{-1} yields amorphous carbon, while $V \approx 10^{6}$–10^{8} K s^{-1} of quenching rate leads to metastable crystalline phases [28].

The low repetition rate of laser corresponding to 12.5 μs pulse duration employed in the present study, moving at a speed of 2×10^{9} nm s^{-1}, hinders the ultra-rapid quenching and promotes slow undercooling, leading to restricted epitaxial growth as observed in high-resolution transmission electron microscope (HRTEM) analysis, shown in figure 4b. The findings in this study in agreement with the study of Sun *et al* [16], where a much longer pulse laser with a pulse width of 1.2 ms has been employed, resulting in the formation of ultrafine nanodiamonds.

Due to a very small 10 μm beam diameter, the final sample obtained was limited with high graphitic content. Therefore, in order to identify the crystal planes associated with diamond, high-resolution XRD was performed on the sample, as shown in figure 3. In XRD spectra the diamond (111) and graphite (110) peaks stay close to each other, to distinguish between the two peaks XRD centred at $2\theta = 44°$ is shown in inset (a). The spectra of laser-ablated sample (in blue) is comprised of a peak at $2\theta = 44°$ reflecting the (111) plane of the diamond. The laser-ablated sample also presented a small peak at $2\theta = 44.2°$, similar to one in the pure graphite sample (in black), suggesting the presence of graphitic content in the sample. Other characteristic planes of diamonds (220), (311), (400) corresponding to $2\theta = 75.4°$, 90.75° and 119.8° can also be seen in the inset (c–e). The diamond peaks are indexed using JCPDS file card no. 750219. It may be noted that a peak centred at $2\theta = 55°$ is also present in the spectra as shown in inset (b). This peak is associated with the (200) plane of the newly discovered 'n-diamond' and is forbidden for diamond [29]. This plane corresponds to the fcc cubic structure of carbon with lattice constant 0.3594 nm, which is quite close to that of diamond thus named n-diamond (new diamond) [30].

The selected area electron diffraction (SAED) pattern in figure 4c also confirms the presence of (200) plane of n-diamond. This is in agreement with the work of Mortazavi and co-workers [30] that the usage of IR laser induces more energetic plasma at solid–liquid interface, leading to the formation of n-diamond, which is generally formed under more extreme temperature and pressure than cubic

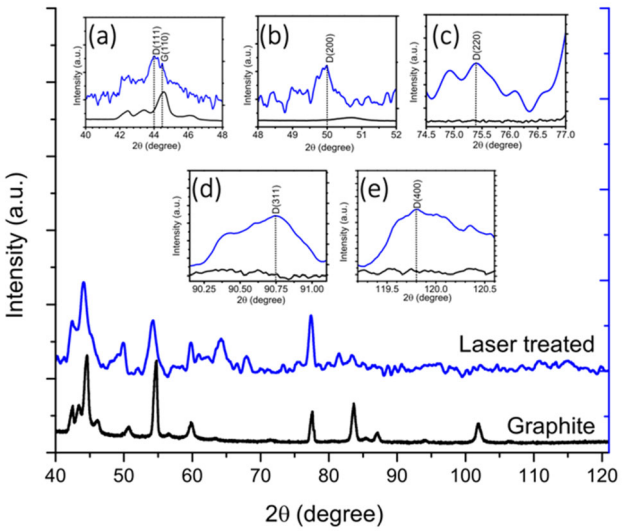

Figure 3. XRD diffractogram of graphite sample (in black) and laser-treated sample (in blue). In inset (**a–e**), high-resolution XRD of laser-treated sample showing diamond planes (111), (200), (220), (311) and (400), corresponding at $2\theta = 44.1$, 50, 75.4, 90.7 and 119.8, respectively.

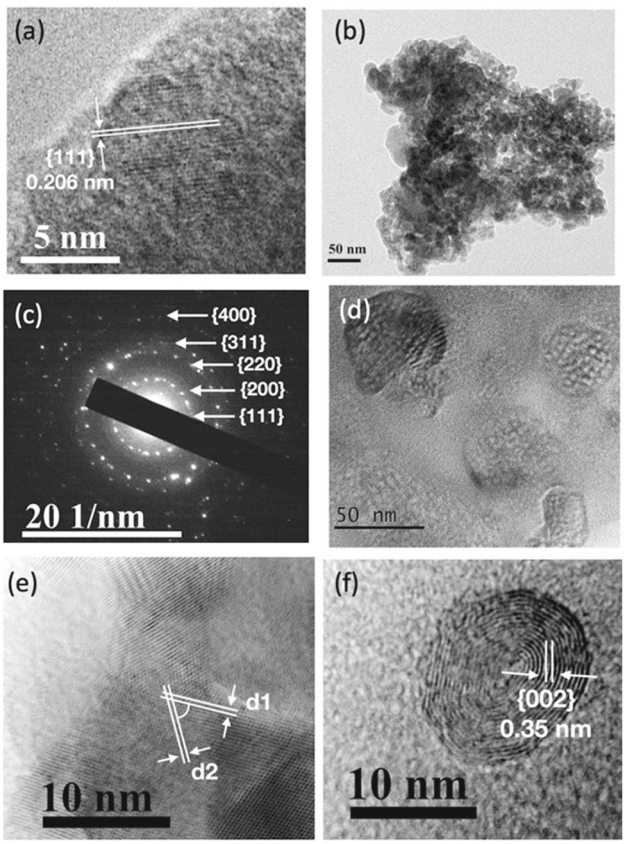

Figure 4. (**a**) HRTEM image of single nanodiamond with interplanar spacing $d = 0.206$ nm. (**b**) HRTEM image of nanodiamonds clusters. (**c**) SAED diffraction of nanodiamonds. (**d**) n-diamonds embedded in amorphous carbon. (**e**) HRTEM image of nanodiamonds sitting together with different interfaces. The measured interplanar distances and angle are $d_1 = 0.258$ nm and $d_2 = 0.255$ nm and $\theta(d_1, d_2) = 61°$. (**f**) HRTEM image of carbon onion with 15 concentric graphite shells having interplanar spacing $d = 0.35$ nm.

diamond. HRTEM image of different morphologies of n-diamond can be seen in figure 4d. The n-diamond crystals are found embedded in the amorphous carbon structure. Similar morphologies have been reported by groups previously using different synthesis techniques [17, 29–32].

Figure 4a shows the HRTEM image of a single nanodiamond embedded in graphitic carbon. The calculated d-spacing d = 0.206 nm from the lattice fringes is in good agreement with the reported interplanar spacing for (111) plane of diamond. Figure 4b displays the aggregated cluster of nanodiamonds. The concentric rings obtained from the SAED pattern matches those with the cubic diamond reflecting the (111), (220), (311) and (400) planes. The strong aggregation of nanodiamonds observed in our case has been previously explained to be due to electrostatic interaction between newly formed diamond crystals in colloidal solutions [33].

Figure 4e displays the lattice fringes from the orientation of different planes of nanodiamonds. The measured interplanar distances and angle, i.e., $d_1 = 0.258$ nm, $d_2 = 0.255$ nm and $\theta(d_1, d_2) = 61°$ can only be attributed to diamond [34]. Furthermore, in the rare instance, we also spotted carbon onions as can be seen in figure 4f. A layer of 15 concentric shells with measured interplanar spacing d = 0.35 nm matches closely with the (002) plane of graphite. These spherical structures reversibly transform in the nanodiamonds during the events of laser irradiation. The concentric shells of graphite act as pressure cells in the transformation of diamond crystals and are found to co-exist with the nanodiamonds [35]. These nanostructures might be formed in our study due to the re-irradiation of the graphitic target repeatedly having diamond structures on the surface.

A typical Raman spectrum of graphite and laser-treated sample is shown in figure 5. The starting material, graphite,

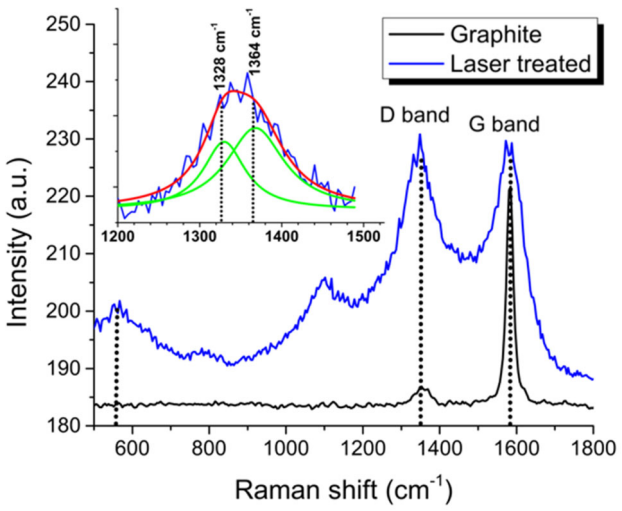

Figure 5. Raman analysis of graphite (black) and laser processed sample (blue). The deconvoluted peaks (green) shown in inset differentiates the diamond peak at 1328 cm^{-1} from graphitic D band.

shows the characteristic G band centred at 1580 cm^{-1} along with the weak D band centred at 1350 cm^{-1}, representing the ordered graphitic layers of sp^2 microdomains and some bond angle-related disorders, respectively [36]. The laser-treated sample reveals diminished G band with a broad feature around the D band. Due to the inherent core-shell structure of nanodiamond, spectral studies are dominated by the graphitic and amorphous structures owing to their larger Raman cross-section for visible excitation [36]. As a result, we deconvoluted this peak centred around 1350 cm^{-1} using Origin Pro software by Origin Lab (version 9.0.0) to distinguish the diamond peak from the D band. We fitted two peaks in the region 1250–1450 cm^{-1} using the Lorentzian multiple peak fitting procedure centred around 1330 and 1360 cm^{-1}. As shown in the inset, the best fit was produced after 3 iterations with Adj R^2 = 0.91506. The resultant first peak centred at 1328 cm^{-1} represents the nanodiamonds, indicating the sp^3 bonding structures. The observed downward shift of the peak from 1332 cm^{-1} for the bulk diamond is due to the phonon confinement effect in crystal sizes lower than ≈10–20 nm [37,38]. In contrast to the large size crystals, where translational symmetry is preserved over large distances, the plane-like waves cannot exist within the nanocrystals due to the finite boundary leading to the confinement of the phonons. It results in the observed peak broadening with a full-width at half-maximum (FWHM) = 46 cm^{-1} along with the downshift of 4 cm^{-1}. Based on this phonon confinement model [37], the relationship between the FWHM of Raman peak and the crystallite size has been taken from the earlier report [39]:

$$\Gamma = 2.990 + 0.185/L, \quad (1)$$

where Γ is the FWHM of the Raman peak (cm^{-1}) and L the particle size (μm). In our case, the measured FWHM of 46 cm^{-1} resulted in the average size of the diamond core around 4.3 nm, which is in good agreement with the HRTEM analysis considering the core-shell morphology of nanodiamond crystals.

The remarkable sensitivity of Raman to molecular morphologies reveals several other spectral features. For example, another peak at 1364 cm^{-1} is due to the presence of short graphitic and amorphous structures in the sample, which is also apparent in figure 4. As compared to the weak D band of the graphite sample (shown in black), the D band of the laser-treated sample is broad and intense reflecting the abundance of these fragments in different sizes. The broad peak around 550 cm^{-1} also indicates the presence of amorphous sp^3 bonded carbon in these structures [40]. Moreover, the diminished G band in the purified sample proves the efficacy of the purification method reported by Pichot *et al* [24] and its broadening reflects the influence of bond bending due to shell curvature of graphitic carbon [41]. It indicates the presence of a curved graphitic outer shell, which is responsible for the epitaxial growth retardation of nanodiamond crystals during the event of rapid quenching. All these evidences suggest that the fibre laser

employed in the present study is propitious to produce fine nanodiamonds.

4. Conclusion

In conclusion, we have demonstrated the applicability of a commercially available low power fibre laser to produce the localized HPHT environment necessary for the generation of diamonds. Despite the low yield of the sample due to the very small 10 μm laser beam diameter, sufficient characterization studies were performed to identify the nanodiamonds with different morphologies. The narrow size distribution found in the study is due to the restricted epitaxial growth of the diamond crystallites within the plasma in the event of rapid quenching. Parameters like laser wavelength and pulse width also play a crucial role in the morphologies and dynamic size of nanodiamond by affecting the localized plasma temperatures and the rate of supercooling, respectively. Considering the ever-increasing demand of nanodiamonds in various sizes and shapes, fibre lasers with different specifications can be utilized and various parameters such as power and repetition rate can be optimized for synthesizing different types of nanodiamond crystals. This synthesis route also proves to be highly environment-friendly and cost-effective, as the raw materials are just deionized water and graphite, while the laser employed is an inexpensive source as compared to other high power pulsed lasers. Moreover, by changing the substrate and solution, variety of other important metastable nanocrystals requiring high activation energy can also be synthesized.

Acknowledgement

We are thankful to Institute of Nano Science and Technology, Mohali, for providing the necessary facilities to carry out the research work.

References

[1] Bormashov V S, Troschiev S Y, Tarelkin S A, Volkov A P, Teteruk D V, Golovanov A V *et al* 2018 *Diam. Relat. Mater.* **84** 41
[2] Kin Y, Saito K, Oda H, Ando T and Nakagawa K 2019 *Catal. Lett.* **149** 1
[3] Prawer S and Greentree A D 2008 *Science* **320** 1601
[4] Batzer M, Shields B, Neu E, Widmann C, Giese C, Nebel C *et al* 2020 *Opt. Mater. Express.* **10** 492
[5] Oh A 2015 *J. Instrum.* **10** C04038
[6] Tinwala H and Wairkar S 2019 *Mater. Sci. Eng. C* **97** 913
[7] Danilenko V V 2004 *Phys. Solid State* **46** 595
[8] Butler J E and Windischmann H 1998 *Mater. Res. Bull.* **23** 22
[9] Askari S J, Chen G C and Lu F X 2008 *Mater. Res. Bull.* **43** 1086
[10] Khachatryan A K, Aloyan S G, May P W, Sargsyan R, Khachatryan V A and Baghdasaryan V S 2008 *Diam. Relat. Mater.* **17** 931
[11] Dolmatov V Y 2007 *Russ. Chem. Rev.* **76** 339
[12] Yang G W, Wang J B and Liu Q X 1998 *J. Phys. Condens. Matter* **10** 7923
[13] Mochalin V N, Shenderova O, Ho D and Gogotsi Y 2011 *Nat. Nanotechnol.* **7** 11
[14] Sumiya H and Irifune T 2007 *J. Mater. Res.* **22** 2345
[15] Bai P, Hu S, Zhang T, Sun J and Cao S 2010 *Mater. Res. Bull.* **45** 826
[16] Sun J, Hu S L, Du X W, Lei Y W and Jiang L 2006 *Appl. Phys. Lett.* **89** 183115
[17] Mortazavi S Z, Parvin P, Reyhani A, Mirershadi S and Bonabi R S 2013 *J. Phys. D: Appl. Phys.* **46** 165303
[18] Amans D, Chenus A C, Ledoux G, Dujardin C, Reynaud C, Sublemontier O *et al* 2009 *Diam. Relat. Mater.* **18** 177
[19] Pearce S R J, Henley S J, Claeyssens F, May P W, Hallam K R, Smith J A *et al* 2004 *Diam. Relat. Mater.* **13** 661
[20] Maia F C B, Samad R E, Bettini J, Freitas R O, Vieira N D Jr and Souza-Neto N M 2015 *Sci. Rep.* **5** 11812
[21] Yang G W 2007 *Prog. Mater. Sci.* **52** 648
[22] Glover T E 2003 *J. Opt. Soc. Am. B* **20** 125
[23] Limpert J, Liem A, Zellmer H and Tünnermann A 2003 *Electron. Lett.* **39** 645
[24] Pichot V, Comet M, Fousson E, Baras C, Senger A, Normand F L *et al* 2008 *Diam. Relat. Mater.* **17** 13
[25] Hoffman J, Chrzanowska J, Kucharski S, Moscicki T, Mihailescu I N, Ristoscu C *et al* 2014 *Appl. Phys. A* **117** 395
[26] Berthe L, Fabbro R, Peyre P and Bartnicki E 1998 *EPJ Appl. Phys.* **3** 215
[27] Harilal S S, Bindhu C V, Issac R C, Nampoori V P N and Vallabhan C P G 1997 *J. Appl. Phys.* **82** 2140
[28] Basharin A Y, Dozhdikov V S, Dubinchuk V T, Kirillin A V, Lysenko I Y and Turchaninov M A 2009 *Tech. Phys. Lett.* **35** 428
[29] Wen B, Zhao J, Li T, Dong C and Jin J 2005 *J. Phys. Condens. Matter* **17** L513
[30] Wen B, Zhao J J and Li T J 2007 *Int. Mater. Rev.* **52** 131
[31] Konyashin I, Zern A, Mayer J, Aldinger F, Babaev V, Khvostov V *et al* 2001 *Diam. Relat. Mater.* **10** 99
[32] Xiao J, Li J L, Liu P and Yang G W 2014 *Nanoscale* **6** 15098
[33] Chang L Y, Ōsawa E and Barnard A S 2011 *Nanoscale* **3** 958
[34] Dunlop A, Jaskierowicz G, Ossi P and Della-Negra S 2007 *Phys. Rev. B* **76** 155403
[35] Xiao J, Ouyang G, Liu P, Wang C X and Yang G W 2014 *Nano Lett.* **14** 3645
[36] Ferrari A C and Robertson J 2001 *Phys. Rev. B* **64** 075414
[37] Richter H, Wang Z P and Ley L 1981 *Solid State Commun.* **39** 625
[38] Osswald S, Mochalin V N, Havel M, Yushin G and Gogotsi Y 2009 *Phys. Rev. B* **80** 075419
[39] Ren X D, Yang L M, Zheng L M, Yuan S Q, Tang S X, Ren N F *et al* 2014 *Appl. Phys. Lett.* **105** 021908
[40] Prawer S, Nugent K W, Jamieson D N, Orwa J O, Bursill L A and Peng J L 2000 *Chem. Phys. Lett.* **332** 93
[41] Obraztsova E D, Fujii M, Hayashi S, Kuznetsov V L, Butenko Y V and Chuvilin A L 1998 *Carbon* **36** 821